15 April 2002

ELSEVIER

Chemical Physics Letters 356 (2002) 14–22

CHEMICAL PHYSICS LETTERS

www.elsevier.com/locate/cplett

Vibrational energy transfer in molecular oxygen collisions

Cecilia Coletti [a], Gert D. Billing [b,*]

[a] *Facoltà di Farmacia, Università "G. D'Annunzio" 66100 Chieti, Italy*
[b] *Department of Chemistry, H. C. Ørsted Institute, University of Copenhagen, DK-2100 Ø,Copenhagen, Denmark*

Received 10 January 2002; in final form 21 January 2002

Abstract

Rate coefficients for the relaxation of vibrational excited oxygen molecules, including both vibration-to-vibration (V–V) and vibration-to-translation (V–T) energy exchange, have been calculated using a semiclassical method and a new potential energy surface for a large interval of initial vibrational quantum numbers ($1 \leqslant v \leqslant 29$) in the temperature range between 50 and 1000 K. © 2002 Published by Elsevier Science B.V.

1. Introduction

The determination of rate coefficients for vibrational energy exchange processes taking place in non equilibrium conditions – i.e., when the local thermal equilibrium assumption is bound to fail – is crucial for the modeling of the population distribution of vibrational and rotational states. These conditions can be the rule in the chemistry of the upper atmosphere, in combustion or laser chemistry, or in plasma chemistry, especially when the vibrations of diatomic molecules are concerned.

The relaxation of highly vibrational excited oxygen molecules ($v \geqslant 8$) is one of the processes having received major attention in this sense due to its great relevance in atmospheric chemistry [1–13]. As a matter of fact this process is a competitor with the reaction between O_2 ($v \geqslant 25$) and O_2 ($v = 0$) proposed as a source of ozone formation in the upper stratosphere and mesosphere, as a suggestion to explain the observed jump in the depletion rates found experimentally for $v \geqslant 26$ [1,12]. Indeed recent papers [8–11] seem to confirm the predominance of the inelastic vibrational relaxation over the above mentioned reaction, although the extent of the experimental quenching is not completely reproduced.

In this Letter a series of rate coefficients are calculated for vibrational relaxation involving vibration-to-vibration (V–V) energy transfer processes

$$O_2(v) + O_2(v' = 0) \rightarrow O_2(v - 1) + O_2(v' = 1) \quad (1)$$

for a wide range of the initial vibrational quantum number v ($1 \leqslant v \leqslant 29$) and of temperature 50 K $\leqslant T \leqslant$ 1000 K, and the vibration-to-translation (V–T) energy exchange process

$$O_2(v) + O_2(v' = 0) \rightarrow O_2(v - 1) + O_2(v' = 0) \quad (2)$$

for the same range of initial vibrational quantum numbers and for 300 $K \leqslant T \leqslant$ 1000 K.

* Corresponding author. Fax: +45-35-320259.
E-mail address: gdb@theory.ki.ku.dk (G.D. Billing).

0009-2614/02/$ - see front matter © 2002 Published by Elsevier Science B.V.
PII: S0009-2614(02)00279-8

Most of the previous works [1–11] concerning the relaxation of highly vibrational excited oxygen molecules were focused on high values of v ($v \geqslant 8$), related, as mentioned before, to the interest for a possible explanation to the sudden increase in the rate of disappearence of vibrational excited O_2, and in particular on the analysis of V–T energy transfer processes which are predominant over the V–V ones for such quantum numbers. However for $v \leqslant 18$ V–V processes mainly determine the global rate of vibrational deactivation for oxygen molecules. Thus some experiments have been recently carried out [14] in order to determine the V–V rate coefficients for low values of v ($v = 2, 3$). In this work we are also concerned with low initial vibrational quantum numbers, however, in order to test the potential energy surface used (see below) we have calculated relaxation rate coefficients up to $v = 29$.

The method used in the present calculation has been developed by Billing [15–17] and used for the generation of large tables of rates [18,19] in a wide temperature interval (larger than that usually achievable experimentally). This approach is based on semiclassical considerations: the vibrations are treated quantum mechanically by close coupling methods and the rotational and relative translational motions of the two molecules are treated classically; the quantum numbers related to the latter are averaged out assuming a Boltzmann distribution of these states.

Such a treatment includes the full dynamical effects of both short and long range contribution to the potential. Moreover the rotational motion of the molecules and the centrifugal stretch coupling are considered via the classical trajectory treatment (see [20] for a detailed comparison between semiclassical first order and state expansion methods).

As noted in previous papers [21,22] in order to get reliable values for the rate coefficients the availability of an accurate potential energy surface (PES) for the system under study is central. In this work we have used a model potential based on a recently published potential energy surface [23] developed to fit scattering molecular beam data [24] and which has been reported to reproduce well other experimental results, such as the second virial coefficient. Unlike other PES (for example the double many-body expansion (DMBE) of [26]) in this model the reactive channel for the formation of ozone is not open. In [11] it was shown that the inclusion of the reactive channel in the potential can give a significant contribution enhancing the V–T rates for $v \geqslant 25$ and thus partially explaining (even if at values of v higher than the experimental ones) the sudden jump in the relaxation rates at such quantum numbers. In this sense the use of a different PES is particularly interesting in order to confirm or refute such results.

Comparison will be also shown with rate coefficients calculated within the same approach but using an older PES [13]: a difference of about one order of magnitude between the corresponding values is reported, those computed with the new PES showing a very good agreement with the experimental results for values of v not affected by the presence of the reactive channel.

2. Method

As mentioned in the previous section the theoretical treatment has been developed in [16,17]: here we will present only a brief summary. For a complete description the reader is referred to the above cited papers.

The degrees of freedom of the system are separated into a quantum and a classical subsystem, describing respectively the vibrations of the O_2 molecules and the translation/rotational motions.

In general the wavefunction for the quantum mechanical part of the system is expanded as a product of Morse eigenfunctions for the isolated molecules: $\phi^0_{v_1}(r_1)\phi^0_{v_2}(r_2)$, where r_1 and r_2 are the vibrational distances of the two oscillators and v_1 and v_2 are the corresponding initial vibrational quantum numbers. The expansion is inserted in the time dependent Schrödinger equation to give a set of coupled equations for the quantum transition amplitudes $a_{vv'}(t)$

$$\begin{aligned} \imath\hbar\dot{a}_{v'_1v'_2}(t) = \sum \Big[& \Big\langle \phi^0_{v'_1}\phi^0_{v'_2}|V(r_1,r_2,t)|\phi^0_{v_1}\phi^0_{v_2}\Big\rangle \\ & + \imath\hbar\Big\langle \phi^0_{v'_1}\phi^0_{v'_2}|H_{\mathrm{Co}}|\phi^0_{v_1}\phi^0_{v_2}\Big\rangle\Big] a_{v_1v_2}(t) \\ & \times \exp\left[\frac{\imath}{\hbar}(E_{v'_1}+E_{v'_2}-E_{v_1}-E_{v_2})t\right], \end{aligned} \tag{3}$$

where v_1', v_2' are the vibrational quantum numbers after the collision.

The second coupling term in Eq. (3) represents the rotational distortion to first order due to the Coriolis centrifugal stretch, which depends on the rotational momenta $j_i(t)$ of the two molecules

$$H_{\mathrm{Co}} = 2\sum_{i=1,2} j_i(t)\frac{\mathrm{d}j_i(t)}{\mathrm{d}t}\frac{1}{m_i\bar{r}_i^3}\frac{\langle\phi^0_{v_i'}|(r_i-\bar{r}_i)|\phi^0_{v_i}\rangle}{E_{v_i}-E_{v_i'}}, \quad (4)$$

where $\bar{r}_i$ is the equilibrium vibrational distance for the ith molecule. The coupling term depends upon time through the time dependence of the coordinates and angles determined from the classical trajectories.

The classical Hamilton equations are solved in an effective potential V_{av} which is the quantum expectation value of the interaction potential. The equations of motion are thus solved by integrating numerically in cartesian coordinates under the constraints $r_i = \bar{r}_i$. The Hamiltonian for the rotovibrational motion is then given by

$$H = \frac{1}{2\mu}(P_x^2+P_y^2+P_z^2) + \sum_i \frac{1}{2m_i}(p_{x_i}^2+p_{y_i}^2+p_{z_i}^2) + \sum_i \lambda_i(r_i^2-\bar{r}_i^2) + V_{\mathrm{av}}(R(t), r_i, \{\Omega(t)\}) \quad (5)$$

with

$$V_{\mathrm{av}} = \langle\Psi|V(R(t), r_i, \{\Omega(t)\})|\Psi\rangle, \quad (6)$$

where μ is the reduced mass.

$$\mu = \frac{(m_{\mathrm{O}}+m_{\mathrm{O}})(m_{\mathrm{O}}+m_{\mathrm{O}})}{m_{\mathrm{O}}+m_{\mathrm{O}}+m_{\mathrm{O}}+m_{\mathrm{O}}} \quad (7)$$

and $\boldsymbol{R}$ is the distance between the two diatoms and $\boldsymbol{p_i}$ and $\boldsymbol{P}$ are the momenta corresponding to the motion of the two oscillators and their relative motion respectively, and $\{\Omega\}$ collectively represents the set of angles $\gamma_1, \varphi_1, \gamma_2, \varphi_2$, where γ_i, ϑ_i define the orientation of the vector $\boldsymbol{r_i}$ in a coordinate system with the z axis along $\boldsymbol{R}$. Since the vibrational motion and the rotovibrational coupling are included in the quantum treatment, the classical part is reduced to a translation/rigid rotor problem. Therefore the Lagrange multipliers λ_i have been introduced [27].

The interaction potential is expanded in power series around the equilibrium distances of the two oscillators up to the second order

$$\begin{aligned} V(R, r_1, r_2, \{\Omega\}) =& V_0(R, \{\Omega\}) + V_{10}(R, \{\Omega\}) \times (r_1-\bar{r}_1) + V_{01}(R, \{\Omega\}) \times (r_2-\bar{r}_2) + V_{11}(R, \{\Omega\}) \times (r_1-\bar{r}_1)(r_2-\bar{r}_2) \\ &+ \frac{1}{2}V_{20}(R, \{\Omega\})(r_1-\bar{r}_1)^2 + \frac{1}{2}V_{02}(R, \{\Omega\})(r_2-\bar{r}_2)^2. \end{aligned} \quad (8)$$

The amplitude $a_{vv'}$ corresponding to a given classical trajectory is obtained by $a_{vv'} = \lim_{t\to\infty} a_{vv'}(t)$. From these quantities average cross-sections can now be obtained

$$\sigma_{v_1',v_2'}(U, T_0) = \frac{\pi\hbar^6}{8\mu(kT_0)^3 I_1 I_2} \times \int_0^{l_{\max}}\int_0^{j_{1\max}}\int_0^{j_{2\max}} \mathrm{d}j_1\mathrm{d}j_2\mathrm{d}l(2j_1+1) \times (2j_2+1)(2l+1)N^{-1}\sum|a_{v_1'v_2'}|^2, \quad (9)$$

where I_i is the moment of inertia for the ith diatom, T_0 is an arbitrary reference temperature – arbitrary because it cancels out in the calculation of the rate constant (see below) – l is the orbital angular momentum, with $l_{\max} = \hbar^{-1}\sqrt{2\mu U}$ and U is the total classical energy: $U = E_{\mathrm{kin}} + E_{\mathrm{rot}_1} + E_{\mathrm{rot}_2} = E - E_{v_1} - E_{v_2}$, where E_{v_1} and E_{v_2} are the vibrational energies of the oscillators in their initial states and N is the total number of trajectories.

Note that the vibrational energy for the state i, according to the anharmonic oscillator model, is approximated by

$$E_{v_i} = \hbar\omega_{ei}(v_i+\tfrac{1}{2}) - \hbar\omega_{ei}x_{ei}(v_i+\tfrac{1}{2})^2 + \hbar\omega_{ei}y_{ei}(v_i+\tfrac{1}{2})^3. \quad (10)$$

The expression of the exothermic rate constant is then given by

$$k_{v_1'v_2'}(T) = \left(\frac{8kT}{\pi\mu}\right)^{1/2}\left(\frac{T_0}{T}\right)^3 \times \int_0^\infty \mathrm{d}\left(\frac{\overline{U}}{kT}\right)\mathrm{e}^{-\overline{U}/kT}\sigma_{v_1',v_2'}(T_0, \overline{U}), \quad (11)$$

where $\overline{U}$ is the symmetrized semiclassical energy [16].

$$\overline{U} = U + \frac{1}{2}\Delta E + \frac{\Delta E^2}{16U} \tag{12}$$

with

$$\Delta E = (E_{v_1'} + E_{v_2'}) - (E_{v_1} + E_{v_2}). \tag{13}$$

The symmetrization scheme used here approximately restores the quantum mechanical detailed balance principle [28].

3. Potential

As pointed out in Section 1 the availability of an accurate potential energy surface is crucial for reliable calculations of rate coefficients.

Previous results [13] within the same approach, which used parameters for the potential taken from the ab initio results of [29], though giving substantially good qualitative agreement with the experiment [2], were found to be too low of about one order of magnitude, especially for small values of v ($v \leqslant 10$). Indeed recent molecular beam studies [23,24] showed that the utilization of the PES of [29] (or of its refined version [30]) failed to reproduce the experimental glory pattern, thus suggesting that the negative area of the isotropic part of the potential should be larger than calculated. Results in the same direction were found by comparison with data for the second virial coefficient [23]. This surface has also been used to study spectral features of the dimer [25]. In the same paper [23] a new potential energy surface was given, obtained by fitting the absolute value of the experimental scattering cross-sections, leading to good agreement with other experimental results. However this model PES assumes that the two diatoms behave like rigid rotors, i.e., there is no dependence on the vibrational distances r_1 and r_2. In order to correctly describe the potential, including the vibrations of diatoms, we have thus used a different model (described below) where the parameters of [23] for the isotropic contribution to the potential were introduced so to reproduce their results for fixed r_1 and r_2.

Our potential consists of a short range part

$$\begin{aligned} V_{\mathrm{SR}} =& C\mathrm{e}^{-\alpha R}\left[\mathrm{e}^{\alpha(1-\epsilon)r_1c_1} + \mathrm{e}^{-\alpha\epsilon r_1c_1}\right] \\ & \times \left[\mathrm{e}^{\alpha\epsilon r_2c_2} + \mathrm{e}^{-\alpha(1-\epsilon)r_2c_2}\right] \\ & - F\mathrm{e}^{-\eta R}\left[\mathrm{e}^{\eta(1-\epsilon)r_1c_1} + \mathrm{e}^{-\eta\epsilon r_1c_1}\right]\left[\mathrm{e}^{\eta\epsilon r_2c_2} + \mathrm{e}^{-\eta(1-\epsilon)r_2c_2}\right], \end{aligned} \tag{14}$$

where the parameters α and η were taken from the corresponding ones in the short range isotropic contribution to the potential of [23], while C and F were chosen in order to fit the above cited potential, and $c_i = \cos\gamma_i$ and $\epsilon = m_{\mathrm{O}}/(m_{\mathrm{O}} + m_{\mathrm{O}}) = 0.5$.

The multipole contribution to the long range potential is

$$\begin{aligned} V_{\mathrm{LR}} =& \frac{3}{2}R^{-5}\Theta(r_1)\Theta(r_2)[1 - 5\cos^2\gamma_1 - 5\cos^2\gamma_2 \\ & - 15\cos^2\gamma_1\cos^2\gamma_2 + 2(\sin\gamma_1\sin\vartheta_1\sin\gamma_2\sin\vartheta_2 \\ & + \sin\gamma_1\cos\vartheta_1\sin\gamma_2\cos\vartheta_2 - 4\cos\gamma_1\cos\gamma_2)^2], \end{aligned} \tag{15}$$

where the quadrupole moment is approximated by

$$\Theta(r_i) = \Theta_0 + \Theta_1(r_i - \overline{r}_i). \tag{16}$$

The dispersion potential due to van der Waals forces is

$$V_{\mathrm{disp}} = -f_6(R)C_6R^{-6}, \tag{17}$$

where the coefficient C_6 is that of [23]. In the latter however the dispersion term of Eq. (17) comes into play only for values of R greater than 6.45 Å. Thus we needed to include a damping function $f_6(R)$, whose explicit expression according to [31] is given by

$$f_6(R) = 1 - \left[\sum_{k=0}^{6}\frac{(\alpha R)^k}{k!}\right]\mathrm{e}^{-\chi R}. \tag{18}$$

$f_6(R)$ tends to unity as $R \to \infty$ and to zero as $R \to 0$. Generally the parameter χ is taken equal to

Table 1
Potential parameters for $O_2 + O_2$

α	3.436 Å^{-1}
C	522.83 eV
η	1.718 Å^{-1}
F	3.243 eV
Θ_0	-2.8325 (kJÅ^5/mol)$^{1/2}$[a]
Θ_1	5 (kJÅ^3/mol)$^{1/2}$[a]

[a] Ref. [32].

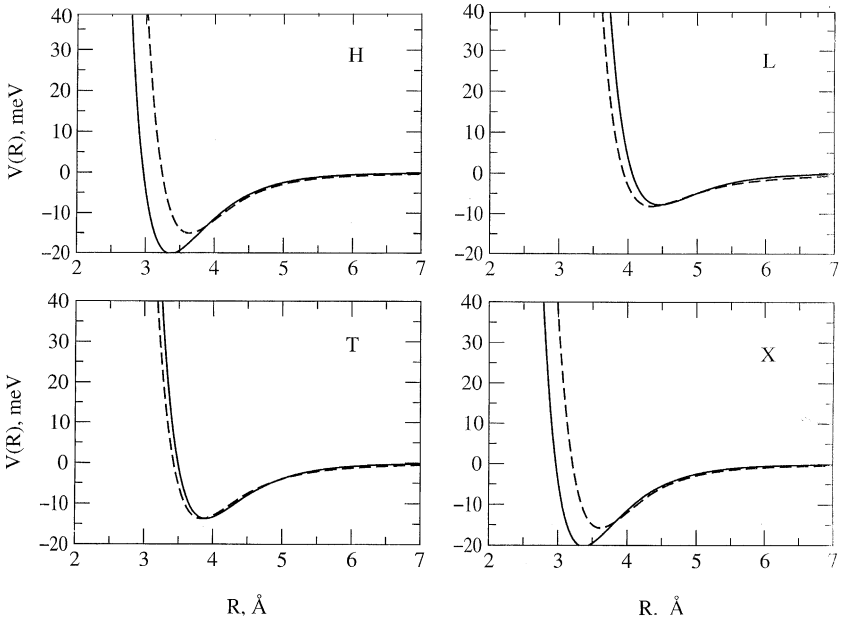

Fig. 1. Potential energy for O_2–O_2 interaction as a function of the distance R between the centers of mass of the diatoms at selected geometries (indicated by H, L, T and X, respectively). The internuclear distances r_1 and r_2 are kept fixed at the equilibrium length. The solid line is obtained using the potential model described in the present work, while the dashed line is the potential of [23]. Unlike [23] our model does not distinguish between the H and X shape.

α of Eq. (14), while here we took $\chi = \alpha/4$ in order to fit the results of [23] and to avoid a too strong damping at large values of R.

Table 1 reports the numerical values of the parameters employed in the calculations while Fig. 1 shows the comparison between our model potential and that of [23] at r_1 and r_2 frozen at their equilibrium distances for some selected geometries.

4. Results

The average cross-sections of Eq. (9), needed to estimate the rate coefficients, have been calculated for 13 values for the classical energy (translational + rotational) in the range 50–75 000 cm^{-1}. The trajectories were started at an intermolecular separation of $R_0 = 15$ Å, and with an impact parameter randomly chosen between 0 and 11 Å. For each energy 500 trajectories have been computed ensuring an accuracy of 20–25% for the V–V cross-sections, while the V–T cross-sections are a little less accurate, especially for low values of v, because of the exiguous number of collisional events leading to V–T energy transfer, thus resulting in poor statistics (as can be seen from the zigzag shape of the V–T curve in Figs. 2 and 3 at low v). For the same reason we have not reported V–T rate coefficients for $T < 300$ K: the initial separation, $R_0 = 15$ Å, could be insufficient to avoid artificial contributions from the long range forces at low energies, thus leading to inaccuracies at low temperature.

The molecular parameters employed in the calculation are listed in Table 2.

Tables 3 and 4 report the rate coefficients for V–V and V–T processes, respectively, for selected temperatures. Fig. 2 shows V–V, V–T and total relaxation constants as a function of v at $T = 300$ K and $T = 465$ K compared with experimental results, while in Fig. 3 comparison is shown with other theoretical results.

Fig. 2 shows a substantial agreement with the experimental results: at 300 K for $v \leqslant 8$ the agreement is very good with [2], while there is a difference of about a factor 2 with the values of [4];

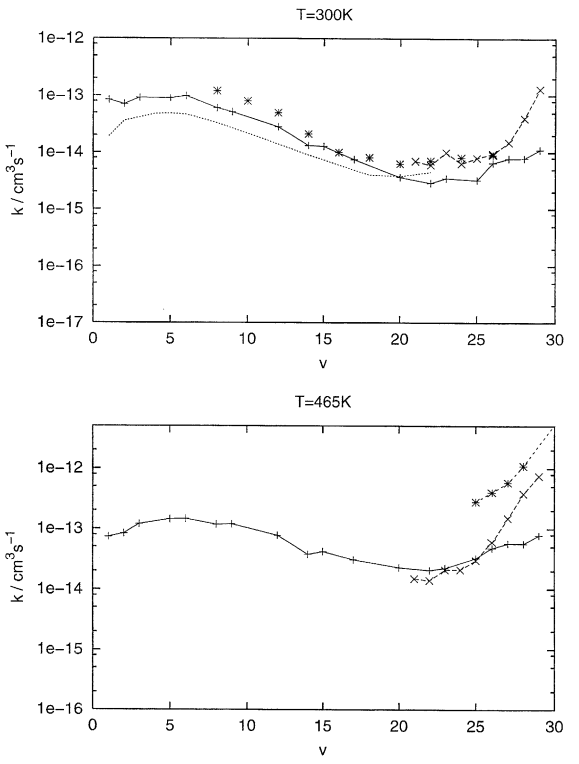

Fig. 2. Calculated V–T (dotted line), V–V (dashed line) and total relaxation rate coefficients (solid line) at $T = 300$ K (upper panel) and at $T = 465$ K (lower panel). Experimental data are also shown for comparison: (∗) [2], (×) [1], (open squares) [4], (filled squares) [6].

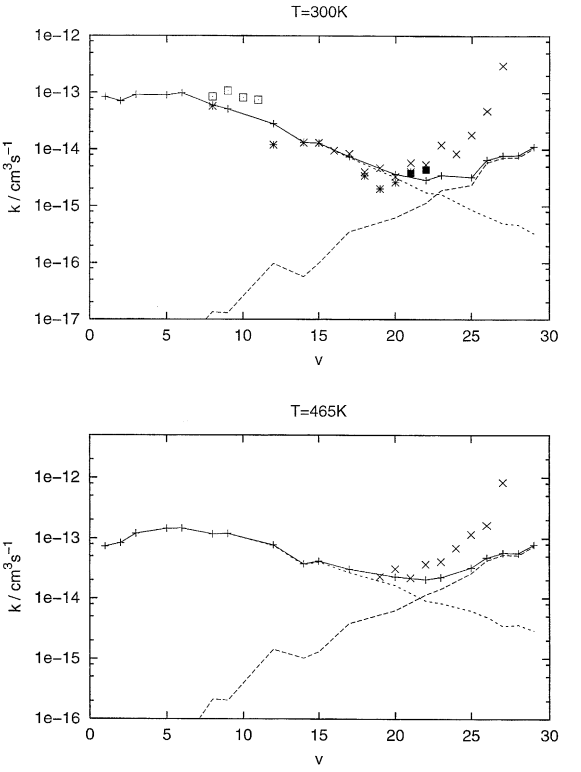

Fig. 3. Comparison between the present calculation (solid line) and other theoretical approaches at $T = 300$ K (upper panel) and $T = 465$ K (lower panel): dashed line (×) [11], (dotted line) [13], (∗) [7], (filled squares) [10].

the comparison with experiments recently carried out for $v = 2$ and $v = 3$ [14] seems to lead to the same underestimation by a factor 2. This difference is however approximately within the accuracy of the method. For $14 \leqslant v \leqslant 23$ the agreement with the experiment is excellent, while at $v > 23$ the calculated values are, as in previous calculations (see also below), noticeably lower than the experimental relaxation rates. The same behavior can be found at 465 K, where the only data available for comparison are above $v = 18$.

Comparison with other theoretical data (Fig. 3) also leads to interesting conclusions. First of all the results obtained in [13] using the same method, but with a different PES are smaller of about one order of magnitude, so that the values presented in this Letter show a much better agreement with the experimental data. This once more verifies the importance of accurate potentials for the modelling of such processes.

Particularly interesting is the comparison with [11] and [10], where the DMBE potential [8] was used, so that the reactive channel is included. This point seems to be extremely important since it was shown that, even if the reaction does not take place, the presence of a saddle point can enhance vibrational energy transfer at highly vibrational

Table 2
Molecular constants for the $^3\Sigma_g^-$ of oxygen [32]

ω_e	1580.3 cm^{-1}
x_e	0.007639
y_e	0.0000345
$\bar{r}$	1.207 Å
β	2.532 $Å^{-1}$

Table 3
V–V rate constants for the process $O_2(v) + O_2(0) \rightarrow O_2(v-1) + O_2(1) + \Delta E$ (ΔE is negative for an endothermic process)

v	ΔE (cm^{-1})	$k_{v,0\rightarrow v-1,1}$				
		100 K	300 K	500 K	700 K	1000 K
1	0.0	1.80E−13	8.44E−14	8.38E−14	9.83E−14	1.26E−13
2	−23.65	4.76E−14	7.10E−14	8.46E−14	8.49E−14	9.97E−14
3	−46.98	4.56E−14	8.99E−14	1.25E−13	1.62E−13	2.28E−13
5	−92.65	3.30E−14	9.03E−14	1.56E−13	2.39E−13	3.80E−13
6	−114.99	2.40E−14	9.85E−14	1.54E−13	2.09E−13	2.94E−13
8	−158.70	6.32E−15	6.08E−14	1.30E−13	2.23E−13	3.95E−13
9	−180.06	3.60E−15	5.52E−14	1.33E−13	2.23E−13	3.71E−13
12	−242.20	5.93E−16	2.81E−14	8.83E−14	1.81E−13	3.56E−13
14	−281.97	2.06E−16	1.32E−14	4.16E−14	8.87E−14	2.05E−13
15	−301.17	1.25E−16	1.27E−14	4.72E−14	1.05E−13	2.24E−13
17	−339.20	6.24E−17	7.17E−15	3.25E−14	8.90E−14	2.28E−13
20	−393.47	6.33E−18	3.17E−15	2.06E−14	6.51E−14	1.89E−13
22	−428.02	4.10E−18	1.73E−15	1.16E−14	3.99E−14	1.31E−13
23	−444.60	1.39E−18	1.60E−15	1.05E−14	3.37E−14	9.90E−14
25	−477.39	1.17E−18	8.76E−16	8.09E−15	2.88E−14	8.24E−14
26	−493.20	1.86E−19	6.65E−16	6.48E−15	2.66E−14	9.24E−14
27	−508.67	5.21E−19	5.04E−16	4.48E−15	1.81E−14	6.42E−14
28	−523.81	1.47E−18	4.73E−16	4.76E−15	1.89E−14	6.07E−14
29	−538.63	3.29E−19	3.32E−16	3.80E−15	1.71E−14	6.16E−14

Table 4
V–T rate constants for the process $O_2(v) + O_2(0) \rightarrow O_2(v-1) + O_2(0) + \Delta E$ (ΔE is negative for an endothermic process)

v	ΔE	$k_{v,0\rightarrow v-1,0}$			
	(cm^{-1})	300 K	500 K	700 K	1000 K
1	1556.3	4.98E−19	8.39E−18	5.77E−17	3.00E−16
2	1532.6	9.10E−19	1.96E−17	1.53E−16	1.14E−15
3	1509.3	1.16E−18	2.83E−17	2.73E−16	1.60E−15
5	1463.7	7.33E−18	8.66E−17	4.33E−16	2.08E−15
6	1441.3	3.88E−18	6.34E−17	5.92E−16	4.14E−15
8	1397.6	1.65E−17	3.38E−16	2.56E−15	1.73E−14
9	1376.3	1.56E−17	3.43E−16	3.02E−15	1.82E−14
12	1314.1	9.74E−17	2.13E−15	1.17E−14	4.98E−14
14	1274.3	6.99E−17	1.65E−15	1.37E−14	7.35E−14
15	1254.9	1.02E−16	2.02E−15	1.39E−14	7.70E−14
17	1217.3	3.57E−16	5.90E−15	3.91E−14	1.91E−13
20	1162.8	6.34E−16	9.78E−15	6.76E−14	3.40E−13
22	1128.3	1.14E−15	1.59E−14	9.18E−14	4.58E−15
23	1111.5	1.53E−15	2.11E−14	3.37E−14	5.10E−13
25	1078.9	2.34E−15	3.48E−14	1.42E−13	5.17E−13
26	1063.1	5.79E−15	5.02E−14	2.98E−13	7.52E−13
27	1047.6	7.16E−15	7.08E−14	3.29E−13	1.13E−12
28	1032.5	7.22E−15	5.18E−14	2.42E−13	9.48E−13
29	1017.7	1.04E−14	9.78E−14	3.78E−13	1.25E−12

excited states. Both papers are thus focused on values of $v \geqslant 21$. Ref. [11] shows that this inclusion indeed increases the relaxation rates, even if this happens at higher values of v and less efficiently than the experiment. This is confirmed by the present calculation: our values, computed neglecting the reactive channel inthe potential, are lower than those of [11] for $v \geqslant 27$.

Note that for $v \geqslant 27$ contributions coming from the asymmetric exchange of vibrational quanta, i.e.

$$O_2(v) + O_2(v' = 0) \rightarrow O_2(v-2) + O_2(v' = 1) \tag{19}$$

have also been added to the total relaxation rates. It was shown [10] that these processes can give a significant contribution to the relaxation coefficients at high values of v, however in our case this contribution is smaller than what was found previously, when the DMBE potential was employed. (In the present work the process (19) accounts for about 1.5% of the total relaxation rate at $v = 27$, about 2% at $v = 28$) and about 2.8% at $v = 29$.) A possible explanation lies again in the inclusion of the saddle point in the above mentioned potential. Since the reaction channel can promote vibrational energy transfer the importance of processes involving multiquantum exchange could also be underestimated if one neglects it.

5. Summary and conclusions

We have calculated a large number of V–V and V–T relaxation rates for the deactivation of vibrational excited molecular oxygen with a semiclassical method and using a recently developed potential energy surface. The method treats the translation and rotation by classical mechanics and only introduces a state expansion in the vibrational modes, so it is very convenient to use for a fast and reliable calculation of these rates. Since only 18 classical equations of motion coupled to a set of time – dependent equations for the vibrational motions (usually less than 100) have to be integrated at a few thousand trajectories the method will run on an ordinary PC computer. This makes it possible to generate large tables of rates.

The agreement with the experimental results is very good up to $v \leqslant 22$ and seems to lead to values approaching recently performed experiments at $v = 2, 3$, while, though showing a sensitive increase, it does not reproduce the sharp jump in the experimental rates at $v \geqslant 25$.

This is again a confirmation that the presence of the reaction channel in the potential favors the possibility of vibrational exchange and thus increases the corresponding rate coefficients. However for smaller values of the initial vibrational quantum numbers the calculated coefficients are very close to the experiment and show an improvement with respect to previous works. A further improvement could be reached by adding to the new PES the anisotropic contributions and spin–spin interactions, present in the original derivation, and which have been neglected here.

Acknowledgements

Dr. Coletti would like to thank Prof. F. Pirani and Dr. D. Cappelletti for useful discussions about the potential energy surface for the system. This research is supported by the Carlsberg Science Foundation and the EU-TMR grant: HPRN-CT-1999-00005.

References

[1] X. Yang, J.M. Price, J.A. Mack, C.G. Morgan, C.A. Rogaski, D. Mc Guire, E.H. Kim, A.M. Wodtke, J. Phys. Chem. 97 (1993) 3944.
[2] H. Park, T.G. Slanger, J. Chem. Phys. 100 (1994) 287.
[3] T.G. Slanger, Science 265 (1994) 1817.
[4] M. Klatt, I.W.M. Smith, R.P. Tuckett, G.N. Ward, Chem. Phys. Lett. 224 (1994) 253.
[5] J.A. Mack, K. Mikulecky, A.M. Wodtke, J. Chem. Phys. 105 (1996) 4105.
[6] K.M. Hickson, P. Sharkey, I.W.M. Smith, A.C. Symonds, R.P. Tuckett, G.N. Ward, J. Chem. Soc., Faraday Trans. 94 (1998) 533.
[7] R. Hernandez, R. Toumi, D.C. Clary, J. Chem. Phys. 102 (1995) 9544.
[8] A.J.C. Varandas, W. Wang, Chem. Phys. 215 (1997) 167.
[9] W. Wang, A.J.C. Varandas, Chem. Phys. 236 (1998) 181.
[10] N. Balakrishnan, A. Dalgarno, G.D. Billing, Chem. Phys. Lett. 288 (1998) 657.
[11] J. Campos-Martinez, E. Carmona-Novillo, J. Echave, M.I. Hernandez, R. Hernandez-Lamoneda, J. Palma, Chem. Phys. Lett. 289 (1998) 150.
[12] R.L. Miller, A.G. Suits, P.L. Houston, R. Toumi, J.A. Mack, A.M. Wodtke, Science 265 (1994) 1831.
[13] G.D. Billing, R.E. Kolesnick, Chem. Phys. Lett. 200 (1992) 382.
[14] T.G. Slanger, Private communication.
[15] G.D. Billing, Chem. Phys. 5 (1974) 244.
[16] G.D. Billing, Comput. Phys. Rep. 1 (1984) 237.
[17] G.D. Billing, Comput. Phys. Commun. 44 (1987) 121.

[18] C. Coletti, G.D. Billing, J. Chem. Phys. 113 (2000) 4869.
[19] Available from http:theochem.ki.ku.dk/~gdb.
[20] G.D. Billing, Int. Rev. Phys. Chem. 13 (1994) 309.
[21] G.D. Billing, Chem. Phys 107 (1986) 39.
[22] C. Coletti, G.D. Billing, J. Chem. Phys. 111 (1999) 3891.
[23] V. Aquilanti, D. Ascenzi, M. Bartolomei, D. Cappelletti, S. Cavalli, M. de Castro Vitores, F. Pirani, J. Am. Chem. Soc. 121 (1999) 10794.
[24] V. Aquilanti, D. Ascenzi, M. Bartolomei, D. Cappelletti, S. Cavalli, M. de Castro Vitores, F. Pirani, Phys. Rev. Lett. 82 (1999) 69.
[25] V. Aquilanti, M. Bartolomei, D. Cappelletti, E. Carmona-Novillo, F. Pirani, Phys. Chem. Chem. Phys. 3 (2001) 3891.
[26] A.J.C. Varandas, A.A.C.C. Pais, in: S.J. Formosinho, L.G. Czismadia, L.G. Arnaut (Eds.), Theoretical and Computational Models for Organic Chemistry, Kluwer, Dordrecht, 1991, p. 55.
[27] G.D. Billing, Chem. Phys. 9 (1975) 359.
[28] G.D. Billing, J. Chem. Phys. 99 (1993) 5849.
[29] P.E.S. Wormer, A. van der Avoird, J. Chem. Phys. 81 (1984) 1929.
[30] B. Bussery, P.E.S. Wormer, J. Chem. Phys. 99 (1993) 1230.
[31] K.T. Tang, J.P. Toennies, J. Chem. Phys. 80 (1984) 3726.
[32] G. Herzberg, Spectra of Diatomic Molecules, Van Nostrand, Princeton, NJ, 1950.